ELSEVIER

Chemical Engineering Journal 93 (2003) 41–53

Chemical Engineering Journal

www.elsevier.com/locate/cej

Gold–ceria catalysts for low-temperature water-gas shift reaction

Qi Fu, Svetlana Kudriavtseva, Howard Saltsburg, Maria Flytzani-Stephanopoulos*

Department of Chemical and Biological Engineering, Tufts University, Medford, MA 02155, USA

Abstract

Nanostructured Au–ceria is a promising new catalyst for low-temperature water-gas shift (LTS). Preparation, characterization, and catalytic properties of this material are reported in this paper. Gold–ceria was prepared by deposition–precipitation (DP), coprecipitation (CP), and gelation methods. The gold loading was varied between 1 and 8.3 at.%, while lanthanum used as a dopant in ceria, was 4 or 10 at.%. Most gold is in metallic state, but ionic gold was also present as identified by XPS. The average ceria crystallite size in samples prepared by gelation was 4.5 and 7 nm, respectively, after calcination at 400 or 650 °C. The gold particle size in samples prepared by DP was <5 nm after 10 h long heating in air at 400 °C. The gold particle size did not increase with gold loading in these samples. A dramatic effect of gold on the reducibility of the surface oxygen of ceria was found by H_2-temperature-programmed reduction (TPR). All of the available surface oxygen was reduced, while there was no effect on the bulk oxygen of ceria. The enhancement of cerium oxide reducibility by gold is independent of the method of catalyst preparation. Oxygen storage capacity (OSC) measurements using step pulses of CO were in agreement with the TPR results; the presence of gold greatly enhances the OSC of ceria. Similar tests with copper-containing ceria were conduced for comparison. Carbon-containing species left on the surface after the CO step, can be fully removed with O_2 or partially removed with H_2O. The high catalytic activity of Au–ceria for LTS reaction correlates well with the ceria structure and oxygen transfer properties.

Keywords: Cerium oxide; Gold; Copper; Water-gas shift; Nanostructured ceria; Oxygen storage capacity

1. Introduction

Fuel cell power generation is currently undergoing rapid development both for stationary and transportation applications. In the transportation sector, fuel cells could replace the internal combustion engines in cars, trucks, buses, etc. while meeting the most stringent emission regulations. In many practical cases, the hydrogen feedstock will be obtained from hydrogen-rich fuels by on-board reforming. Generally, the reformate gas will include H_2, CO and CO_2, H_2O and a small amount of CH_4. However, carbon monoxide needs to be completely removed upstream of a low-temperature fuel cell, such as the PEM fuel cell, not only because it is a criterion pollutant, but also because it poisons the anode catalyst, thus degrading the fuel cell performance. Low-temperature water-gas shift (LTS) is used to convert carbon monoxide with water vapor to hydrogen and CO_2. Potentially, development of a highly active LTS catalyst would obviate the need for the preferential CO oxidation reactor, currently envisioned as the last fuel-processing step upstream of the fuel cell anode. Desired catalyst characteristics include high activity and stability over a wider operating temperature window than is currently possible with the commercial LTS catalysts.

Catalysts based on cerium oxide are promising for this application [1,2]. Ceria is presently used as a key component of the three-way catalyst in automotive exhausts. Ceria is also a good choice as a support of both noble metal and base metal oxide catalysts, participating in redox reactions by supplying oxygen. Metal–ceria systems are several orders of magnitude more active than metal/alumina or other oxide supports for a number of redox reactions [2–4]. Sanchez and Gazquez [5] proposed that oxygen vacancies in the fluorite oxide structure in supported catalysts alter the morphology and dispersion of the supported metal. Metal-modified cerium oxide has a higher oxygen storage capacity (OSC) and reducibility than pure ceria [1,6,7]. We have recently reported that Cu–ceria is more stable than other Cu-based LTS catalysts and at least as active as the precious metal–ceria systems, which are well known for their LTS activity in the catalytic converter [2].

In this paper, we report on the Au–(La doped) ceria system as an LTS catalyst. During the past decade, many studies have established that nanosized Au-on-reducible oxides have a remarkable catalytic activity for many important oxidation reactions, especially low-temperature CO oxidation, WGS, HC oxidation, NO reduction and the selective oxidation of propylene to propylene oxide [8–10,12–17]. There is

* Corresponding author. Fax: +1-617-627-3991.
E-mail address: maria.flytzani-stephanopoulos@tufts.edu (M. Flytzani-Stephanopoulos).

1385-8947/02/$ – see front matter
PII: S1385-8947(02)00107-9

presently no consensus as to the cause of the very high activity of nanoparticles of Au-on-reducible oxides. For example, in oxidation/reduction reactions, some researchers have argued that the oxygen at the interface between the metal and the oxide support is important [8,18], while others invoke dissociative O_2 adsorption on very small Au particles in atomic state [19,20] but not on bulk Au particles to explain the activity. The unique properties of supported nanoscale Au have been correlated to a number of variables, including Au particle size [19], Au–support interface [8], the state and structure of the support [14,21], as well as the pretreatment of catalysts [18]. Preparation methods have been given due attention. Two commonly used methods are coprecipitation (CP) and deposition–precipitation (DP). The conventional solution impregnation method cannot be used to obtain active gold catalysts [8] unless it is followed by a certain heat treatment involving both reducing and oxidizing gases [18].

In this work, we prepared nanoscale Au–(La doped) ceria catalysts using three different techniques: CP, DP, and urea gelation/coprecipitation (UGC). We report on the WGS activity of Au–ceria catalysts and compare them to Cu–ceria catalysts. The WGS activity is further correlated to the catalyst structure and oxygen transfer properties.

2. Experimental

2.1. Catalyst preparation

Doped and undoped bulk ceria was prepared by the UGC method, as described in detail elsewhere [1]. The cerium salt used in UGC is $(NH_4)_2Ce(NO_3)_6$. In brief, aqueous metal nitrate solutions were mixed with urea ($H_2N–CO–NH_2$) and heated to 100 °C under vigorous stirring and addition of deionized water. The resulting gel was boiled and aged for 8 h at 100 °C; after aging, the precipitate was filtered and washed with deionized water until there were no residual Cl^- ions as tested by $AgNO_3$ solution. Further, the precipitate was dried at 100–120 °C and calcined in static air at 400 °C for 10 h or 650 °C for 4 h. A heating rate of 2 °C/min to the selected temperature was used. In all preparation methods used in this work, the precipitate was treated by the same procedures.

In the studies of Au–ceria reported by Liu and Flytzani-Stephanopoulos [9], a CP method using ammonium carbonate as the precipitant was used to prepare the catalyst. More recently, Weber [22] studied various preparation methods and conducted a full parametric study of each method in an effort to optimize the activity of this catalyst for CO oxidation. A DP technique was found the most promising. Both of these methods were used here while the UGC was also used to prepare one Au–ceria sample and Cu–ceria samples for comparison.

CP involves mixing an aqueous solution of $HAuCl_4$, cerium(III) nitrate and lanthanum nitrate with $(NH_4)_2CO_3$ at 60–70 °C, keeping a constant pH value of 8 and aging the precipitate at 60–70 °C for 1 h. For DP [22,23], the ceria support was first prepared by UGC and calcined. DP took place by adding the desired amount of $HAuCl_4$ dropwise into aqueous slurry of the prepared ceria. The pH of the aqueous slurry had already been adjusted to the value of 8 using $(NH_4)_2CO_3$. The resulting precipitate was aged at room temperature (RT) for 1 h. It should be noted that unlike a previously reported DP method [24] which uses NaOH as the base and excess (about five times) $HAuCl_4$, the present method can deposit the desired gold loading on ceria using the exact amount of $HAuCl_4$ solution [22].

For comparison to Au–ceria samples prepared by CP and DP, one sample containing a large loading (8 at.%) of gold in ceria was prepared by UGC, but the solution containing $HAuCl_4$, $(NH_4)_2Ce(NO_3)_6$, $La(NO_3)_2$ and urea, was heated to 80 °C instead of 100 °C. Both bulk copper–ceria samples used in this work were made by UGC, following the procedure described above for metal-free ceria.

All reagents used in catalyst preparation were analytical grade. The samples reported here are denoted as αAu–CL(z), where α is the at.% gold loading $[100 \times (Au/M_{Au})/(Au/M_{Au} + Ce/M_{Ce} + La/M_{La})]$ and z is the method of preparation: CP, DP, or UGC. Calcination temperature will be noted only if it differs from 400 °C, the typical catalyst calcination temperature used for most samples. The lanthanum doping of ceria is around 10 at.%. These samples are denoted as CL.

2.2. Catalyst characterization

The bulk elemental composition of each sample was determined by inductively coupled plasma (ICP) atomic emission spectrometry (Perkin-Elmer, Plasma 40). The total sample surface area was measured by single-point BET N_2 adsorption/desorption on a Micromeritics Pulse ChemiSorb 2705.

X-ray powder diffraction (XRD) analysis of the samples was performed on a Rigaku 300 X-ray diffractometer with rotating anode generators and a monochromatic detector. Cu Kα radiation was used. The crystal size of ceria and gold was calculated from the peak broadening using the Scherrer equation [25].

High-resolution transmission electron microscopy (HRTEM) was used to study the sample morphology. The analyses were performed on a JEOL 2010 instrument with an ultimate point-to-point resolution of 1.9 Å and lattice resolution of 1.4 Å. The TEM was equipped with a X-ray detector for elemental analysis of selected samples areas. The sample powder was suspended in isopropyl alcohol using an ultrasonic bath and deposited on the carbon-coated 200 mesh Cu grid.

A Kratos AXIS Ultra Imaging X-ray photoelectron spectrometer with a resolution of 0.1 eV was used to determine the atomic metal ratios of the surface region and metal oxidation state of selected catalysts. Samples were in powder form and were pressed on a double-side adhesive copper tape. All measurements were carried out at RT without any

sample pretreatment. An Al Kα X-ray source was used in this work.

2.3. Activity tests

Water-gas shift reaction tests were performed at atmospheric pressure with 150 mg catalyst powder (50–150 μm size). The catalyst was supported on a quartz frit at the center of a quartz-tube flow reactor (1.0 cm i.d.), which was heated inside an electric furnace. The feed gas mixture typically contained 2% CO and 10.7% H_2O in helium. The total gas flow rate was 100 cm^3/min (NTP). The corresponding contact time for the ceria-based samples was 0.09 g s/cm^3 (gas hourly space velocity, GHSV = 80,000 h^{-1}). All ceria samples were used in the as prepared form without activation. Water was injected into the flowing gas stream by a calibrated syringe pump and vaporized in the heated gas feed line before entering the reactor. A condenser filled with ice was installed at the reactor exit to collect water. The reactant and product gas streams were analyzed using a HP-6890 gas chromatograph equipped with a thermal conductivity detector (TCD). A Carbosphere (Alltech) packed column (6 ft × 1/8 in.) was used to separate CO and CO_2.

2.4. Temperature-programmed reduction (TPR)

TPR of the as-prepared catalysts in fine powder form was carried out in a Micromeritics Pulse ChemiSorb 2705 instrument. The samples were first oxidized in a 10% O_2/He gas mixture (50 cm^3/min (NTP)) at 350 °C for 30 min, cooled down to 200 °C and then flushed with pure nitrogen (Grade 5) to RT. The sample holder was then immersed in liquid nitrogen. A 20% H_2/N_2 gas mixture (50 cm^3/min (NTP)) was next introduced over the sample causing a large desorption peak, at the end point of which the liquid N_2 was removed and the sample temperature was raised to RT. A second large desorption peak was recorded at that time. Those two peaks appeared with all samples, even for pure ceria, and were identical; thus, they are attributed to desorption of physically adsorbed nitrogen and hydrogen. The sample was then heated at a rate of 5 °C/min from RT to 900 °C. A cold trap filled with a mixture of isopropanol and liquid nitrogen was placed in the gas line upstream of the TCD to remove the water vapor.

2.5. OSC measurements

OSC measurements were carried out in a flow reactor system, equipped with a switching valve for rapid introduction of step changes in gas streams of CO/He, He, and O_2/He. Catalyst samples were prepared by cold pressing thin disks from powders and breaking the disks into small pieces. The fragments (0.3 g) were loaded into the (1/4) in. quartz reactor tube and supported on a frit. A total gas flow rate of 50 cm^3/min (NTP) was used. Certified gas mixtures were used and passed through moisture and oxygen traps before entering the system. The 10% CO/He gas stream passed through a hydrocarbon trap in addition to the above treatments.

The steady-state signals of CO, CO_2 and O_2 were detected by an on-line quadrupole residual gas analyzer (MKS-model RS-1). The reactor tube could be bypassed. Prior to an OSC measurement, the sample was first heated in 10% O_2 at 350 °C for 15–20 min. The sample was further purged in helium in 600 °C for half hour to remove oxygen from the system. Then the sample was exposed to 10% CO/He and 10% O_2/He step changes at the desired test temperature. In all cases, CO_2 production was limited, although CO and O_2 were at initial gas levels. Each experiment consists of flowing CO through the by-pass line for 3 min followed by flowing CO through the reactor for 3 min; then O_2 flowed through the by-pass line for 3 min followed by O_2 flowing through the reactor for 3 min. A 6 min pulse of He between the CO and O_2 step pulses was used to ensure complete removal of gas phase species. The CO flow through the by-pass was used as a blank to stabilize the MS, while the by-pass O_2 was used to remove any carbon deposited on the filament of the mass spectrometer. Integration of the partial pressure as a function of time was used to accurately determine the amounts of CO_2 formed, and CO and O_2 consumed during the CO and O_2 step pulses.

3. Results and discussion

3.1. Catalyst characterization

Au–ceria samples prepared by different techniques had a different crystal habit. These data were reported in detail elsewhere [11,22]. For example, in samples prepared by CP, ceria has a needle-like and layered bulk structure, while in the DP samples, it has a uniform spherical structure, a result of its prior synthesis by the UGC method. A uniform distribution of gold on ceria was found for the DP sample, while the CP sample contained relatively large gold particles with a lower dispersion. This difference between DP and CP methods was also found for gold deposited on several other oxides [14]. Metallic gold was present in both samples [22]. From HRTEM analysis, as shown in Fig. 1, we found that the gold particles in the DP sample have an average size of 5 nm, while the ceria particles are around 7 nm, which is in good agreement with the particle sizes measured by XRD, as shown in Table 1.

XRD patterns from samples prepared by different methods are shown in Fig. 2. These show the presence of CeO_2 and metallic gold crystal phases, which agrees with the STEM/EDS analysis [11,22]. The distinct fluorite oxide-type diffraction pattern of CeO_2 was observed in all samples. Lanthana forms an oxide solid solution with ceria, so there are no separate reflections from La compounds, in agreement with previous work [1,9]. The addition of La inhibits the crystal growth of ceria made by either the CP or the

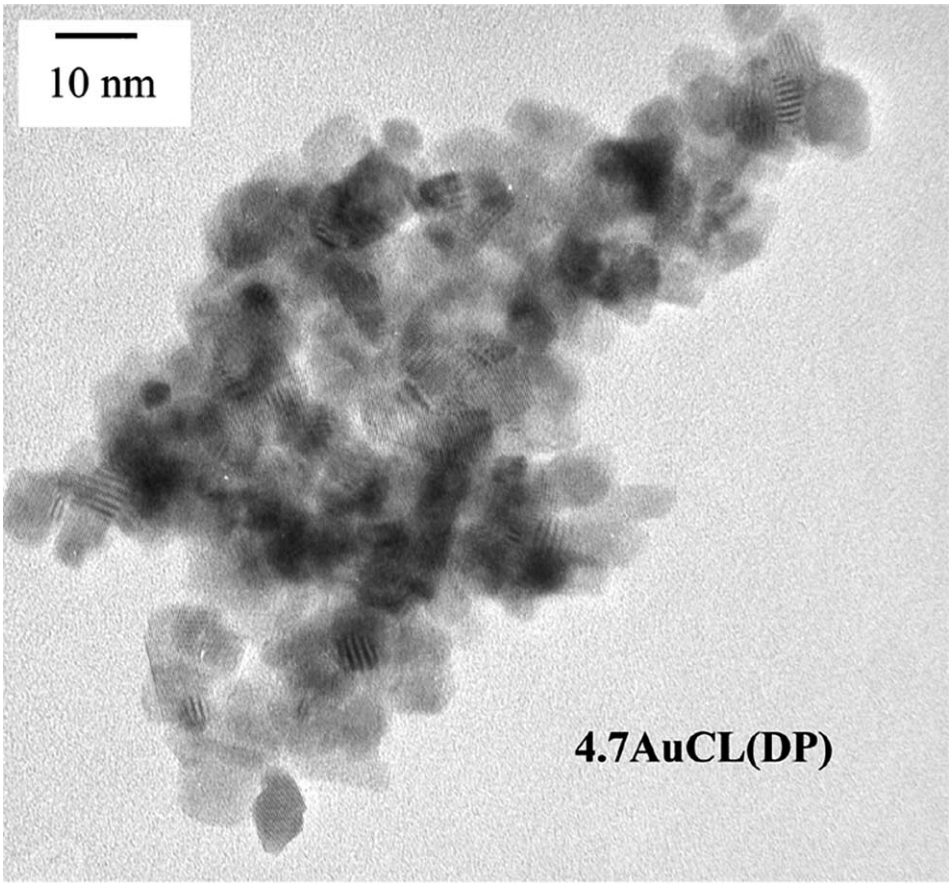

Fig. 1. HRTEM micrograph of 4.7Au–CL (DP) (footnote ‘c’ in Table 1). See Table 1 for sample identification and preparation conditions.

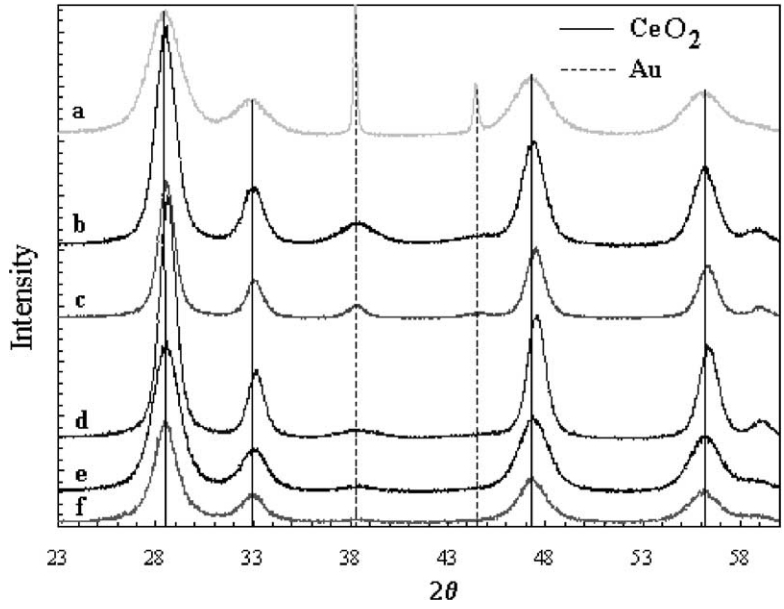

Fig. 2. XRD patterns of Au–ceria samples: (a) 8Au–CL (UGC); (b) 8.3Au–CL (DP) (footnote ‘c’ in Table 1); (c) 4.7Au–CL (DP) (footnotes ‘c’ and ‘d’ in Table 1); (d) 4.7Au–CL (DP) (footnote ‘c’ in Table 1); (e) 4.5Au–CL (DP) (footnote ‘f’ in Table 1); (f) 3.8Au–CL (CP). See Table 1 for sample identification and preparation conditions.

Table 1
Physical properties of ceria-based materials[a]

Sample	BET surface area (m^2/g)	Particle size[b] (nm)		
		Au⟨1 1 1⟩	Ce⟨1 1 1⟩	Ce⟨2 2 0⟩
8.3Au–CL (DP)[c]	93.6	4.5	7.1	6.9
4.7Au–CL (DP)[c,d]	–	9.2	7.1	6.9
4.7Au–CL (DP)[c]	82.7	4.6	7.1	6.9
	71.6[e]	6.8	7.3	7.2
0.9Au–CL (DP)[c]	96.7	–	7.1	6.9
4.5Au–CL (DP)[f]	155.8	5.0	5.2	4.9
3.8Au–CL (CP)	71.8	6.7	5.8	5.3
0.9Au–CL (CP)	102.2	NM[g]	NM	NM
8Au–CL (UGC)	158.1	49.1, 36.6[h]	4.5	4.5
5Cu–CL (UGC)[d,i]	89.1	–	5.2	4.9
5Cu–CL (UGC)[i]	187.1	–	4.0	3.5
10Cu–CL (UGC)[i]	200.3	–	3.5	3.1
CL (CP)	72.2	–	7.4	7.0
CL (CP)[c]	48.0	–	11.6	9.9
CL (UGC)	161.6	–	5.1	4.8
CL (UGC)[c]	93	–	7.1	6.9
CeO_2[j]	78.6	NM	NM	NM

[a] All materials were calcined at 400 °C for 10 h, unless otherwise noted.
[b] Determined by XRD using Scherrer equation.
[c] CL calcined at 650 °C in air.
[d] Sample calcined at 650 °C in air.
[e] Used in 7% CO–38% H_2O–11% CO_2–33% H_2–He for 120 h.
[f] CL calcined at 400 °C in air.
[g] Not measured.
[h] Au⟨2 0 0⟩.
[i] No copper compounds detected by XRD.
[j] La-free, precipitated with ammonium carbonate.

UGC methods [26,27]. The average gold and ceria crystallite sizes, determined by XRD using the Scherrer equation, are listed in Table 1. With increasing calcination temperature, the particle size of ceria and gold increased and the specific surface area decreased. Since gold was deposited on the UGC precalcined ceria in the DP samples, the addition of gold should have no effect on the size and structure of ceria. This is what was found, as can be seen in Table 1 by comparing the crystallite size of ceria before and after the deposition of gold. However, for the CP and UGC samples, the incorporation of gold or copper during the synthesis step may suppress the growth of ceria crystallites during calcination [28], as can be seen in Table 1. This effect has also been reported for Au/Fe_2O_3 [29–31]. Sze et al. proposed that Au could substitute into the Fe_2O_3 unit cell as ions in the +3 state as evidenced by XPS and Mossbauer spectroscopy [29]. Haruta et al. [31] explained that an intermetallic bond is formed between Fe and Au, as supported by the slight solubility Fe in Au and the Au–Fe distance.

In Fig. 2, a small broad peak corresponding to Au(1 1 1), and a barely visible peak corresponding to Au(2 0 0) are seen in all samples, except 0.9Au–CL (DP), which has a very low gold loading. With increasing gold loading, the gold diffraction peak is more pronounced, but the full width at half peak maximum (FWHM) remains unchanged. Thus, the gold particle size does not increase with loading. This indicates a strong interaction between gold and ceria.

When the 4.7Au–CL (DP) sample was calcined at 650 °C, the gold particle size grew to 9.2 nm (Table 1), which is twice the size of the sample calcined at 400 °C (4.6 nm). Thus, there is a significant effect of calcination temperature on the growth of gold particles [24]. Fig. 2 also shows reflections from sample 8Au–CL (UGC), which was prepared by UGC, as described above. The peaks corresponding to Au(1 1 1) and Au(2 0 0) are large and sharp, with a corresponding average gold particle size of 43 nm (Table 1). The ceria particle size, however, was very small (4.5 nm), even smaller than that of CL made by the same gelation method at 400 °C.

The nature of the active gold site is unclear. Haruta and co-workers [8,13,14] have suggested that the active species are small metallic gold particles. In single-crystal studies, Valden et al. [19] found that for catalytic activity, metallic gold is indispensable. However, the catalytic activity can be further enhanced by keeping the electronic structure of gold at the boundary of the transition between ionic and metallic character caused by a strong interaction between the metal and support along the perimeter interface. Other groups [16,32–35] have suggested that both metallic gold and oxidized gold species are responsible for the catalytic oxidation of CO and that oxidized gold species have a much higher activity than metallic gold. Kang and Wan [32] proposed that the most active sites are made of gold hydroxide surrounded by iron oxide. Moreover, Park and Lee [36] suggested that the suppression of the transition from oxidized gold to the less active metallic gold by water is the reason for the substantially higher rates of CO oxidation in wet conditions than in dry conditions, which was also reported by Haruta et al. [37] and Boccuzzi and Chiorino [38].

In this work, the metal oxidation state of selected catalysts was investigated by XPS. The Au 4f and Ce 3d XP spectra of 4.5Au–CL (DP), 3.8Au–CL (CP) and 8Au–CL (UGC) are shown in Fig. 3. Since the C 1s peak from adventitious hydrocarbon present on the samples was found all measurements, it was used as internal standard for the charge correction. Therefore, all the binding energies were adjusted to the C 1s peak of carbon at 284.6 eV. Ce 3d spectra are similar to the standard CeO_2 spectra, showing well resolved Ce^{4+} lines. The gold species identified by the corresponding binding energy [36,39] are shown in Fig. 3B. We found that while most of gold is metallic after the 400 °C air calcination step, part of gold remains ionic in these catalysts. The samples made by UGC and CP have the most oxidic gold [28]. This might suggest that the gelation or CP method can achieve a stronger metal–support interaction to stabilize gold ions. It is interesting to note that the catalyst color is indicative of the proportion of metallic gold. The more metallic gold, the darker the catalyst.

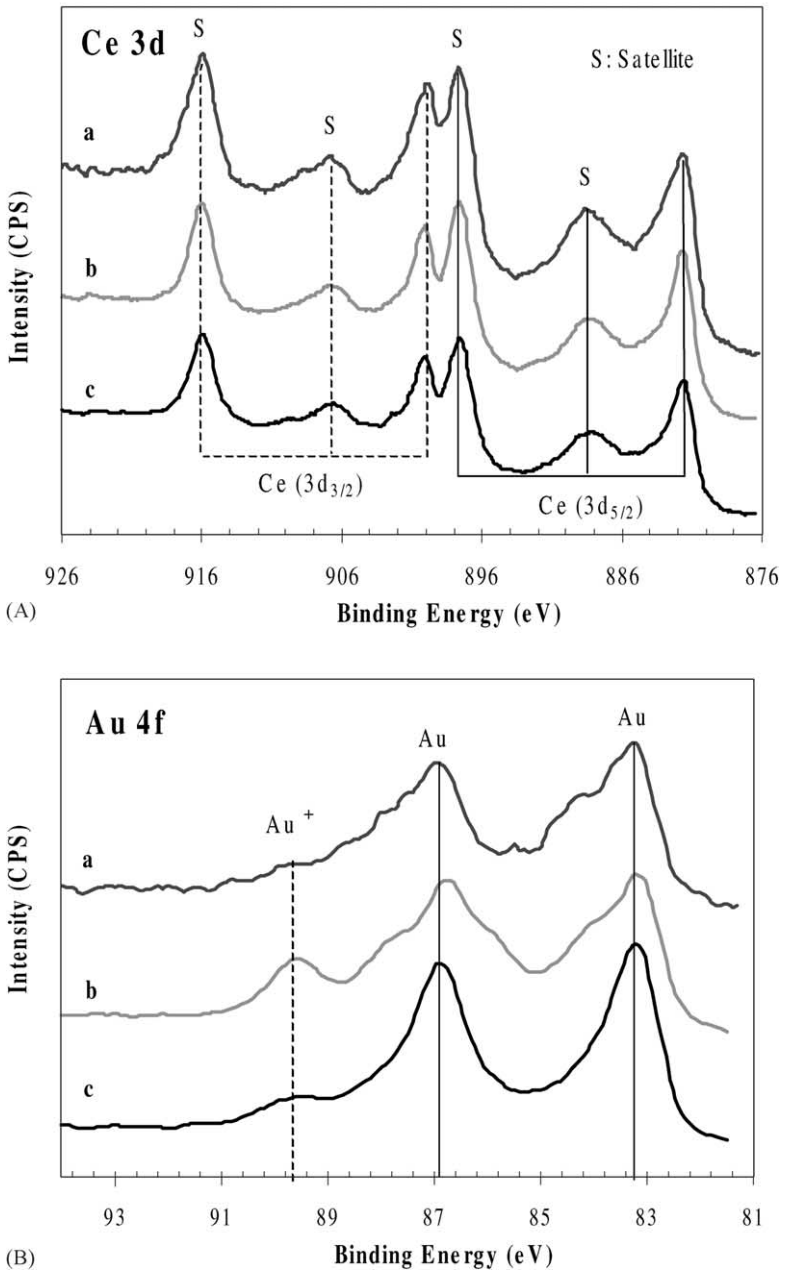

Fig. 3. XP spectra of Au–ceria samples: (A) Ce 3d; (B) Au 4f ((a) 4.5Au–CL (DP) (footnote 'f' in Table 1), (b) 8Au–CL (UGC), (c) 3.8Au–CL (CP)). See Table 1 for sample identification and preparation conditions.

3.2. H_2-TPR and OSC measurements

H_2-TPR of several CL (UGC or CP), Cu–CL and Au–CL (DP or CP) samples was examined in this work. Fig. 4 shows the hydrogen consumption by some of these materials. The reduction peak temperature and corresponding hydrogen consumption are listed in Table 2. The key finding from this analysis is that the surface oxygen of ceria is substantially weakened by the presence of gold and copper nanoparticles, its reduction temperature lowered by several hundred degrees. Exactly how much weaker this oxygen becomes depends strongly on the preparation method, type of metal, metal loading, and calcination temperature.

The onset and amount of oxygen reduction for the CL samples depends on the preparation method, as shown in Fig 4A. CL (UGC) calcined at 400 °C, began to reduce at 350 °C with a peak at 487 °C, which is assigned to the surface capping oxygen of CeO_2 [6]. CL (UGC) calcined at 650 °C has the same reduction profile, but a much smaller peak area, attributed to the lower surface area of this sample. Chiang et al. [40] reported that high surface area ceria has a lower reduction enthalpy than that measured for the bulk

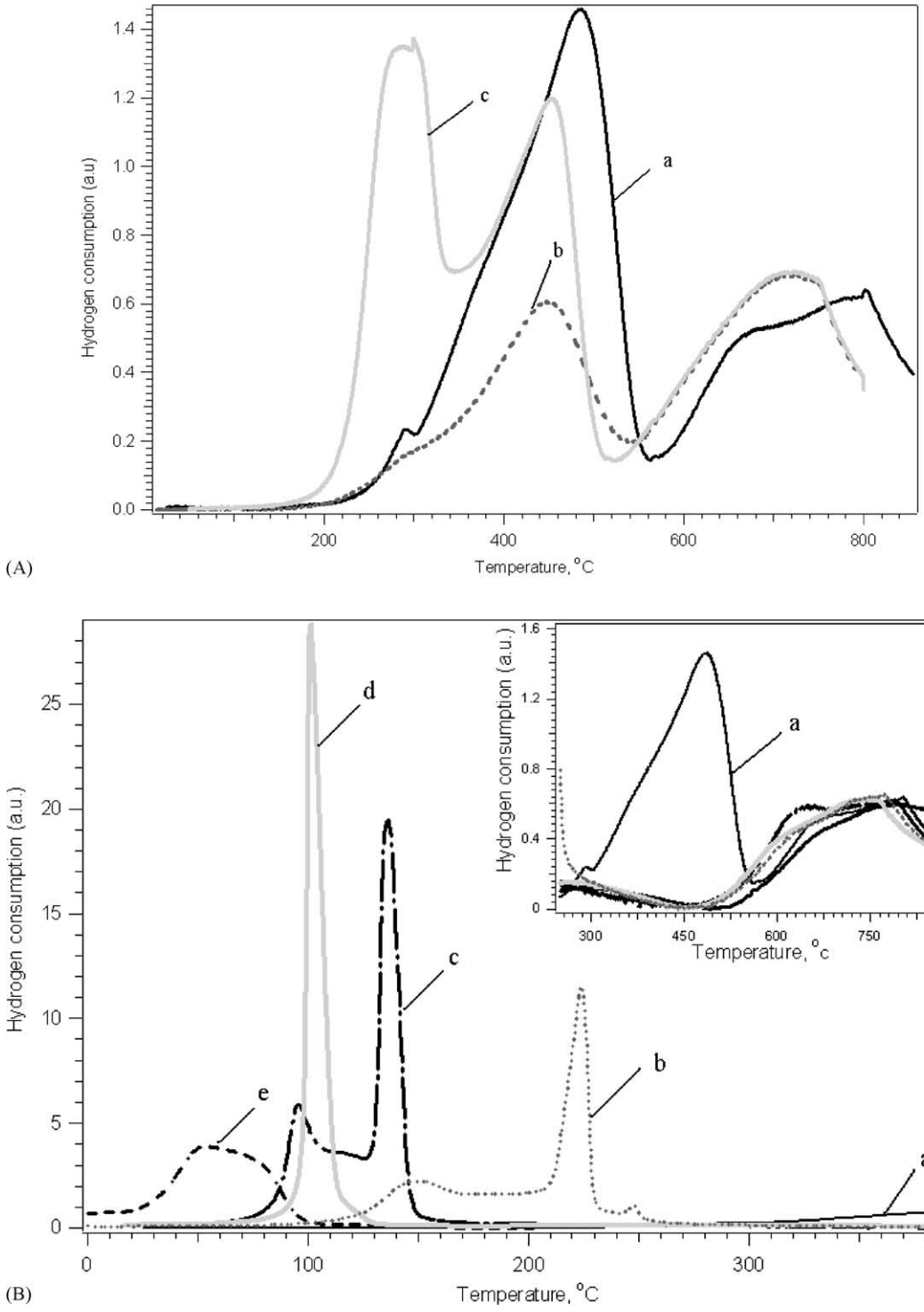

Fig. 4. H_2-TPR profiles of ceria-based samples; 20% H_2/N_2, 50 cm^3/min (NTP), 5 °C/min: (A) (a) CL (UGC) calcined at 400 °C, (b) CL (UGC) calcined at 650 °C, (c) CL (CP) calcined at 400 °C; (B) (a) CL (UGC), (b) 5Cu–CL (UGC), (c) 10Cu–CL (UGC), (d) 8Au–CL (UGC), (e) 4.5Au–CL (DP), all materials calcined at 400 °C, 10 h.

material. Trovarelli and co-workers [7,41] have reported that reduction of ceria strongly depends on the ceria crystallite size. CL (CP) calcined at 400 °C shows two reduction peaks for surface oxygen, one at 310 °C and a second at 497 °C. The latter is at the same position as for CL made by UGC. The first peak maybe due to the interaction of lanthanum with ceria as reported by Groppi et al. [42] for the ternary $CeO_x/LaO_x/Al_2O_3$ material. This is also supported by the absence of a first reduction peak at 310 °C in the TPR profile (not shown) of undoped ceria made by precipitation with

Table 2
H_2-TPR of ceria-based materials[a]

Sample	H_2 consumption (μmol/g_{cat})			"x" in CeO_x (H_2 consumption up to 500 °C)
	Peak 1 (T, °C)	Peak 2 (T, °C)	Peak 3 (T, °C)	
0.9Au–CL (DP)[b]	165 (69)	329 (109)		1.90
4.7Au–CL (DP)[b]	213 (51)	198 (68)		1.92
4.7Au–CL (DP)[b,c]	132 (84)	289 (107)		1.91
8.3Au–CL (DP)[b]	98 (40)	306 (59)		1.91
4.5Au–CL (DP)[d]	560 (55)	192 (79)		1.85
3.8Au–CL (CP)	803 (96)			1.84
0.9Au–CL (CP)	672 (160)			1.87
8Au–CL (UGC)	903 (110)			1.81
5Cu–CL (UGC)[c,e]	275 (126)	282 (132)	175 (145)	1.92
5Cu–CL (UGC)[e]	633 (150)	396 (224)	39 (246)	1.85
10Cu–CL (UGC)[e]	334 (97)	312 (117)	730 (140)	1.85
CL (CP)	431 (310)	455 (497)		1.83[f]
CL (UGC)	706 (487)			1.87[f]
CL (UGC)[b]	425 (437)			1.92[f]
CeO_2[g]	782 (405)			1.87[f]

[a] In 20% H_2/N_2 gas mixture (50 cm^3/min (NTP)), 5 °C/min; all materials were calcined at 400 °C, 10 h, unless otherwise noted.
[b] CL calcined at 650 °C in air.
[c] Sample calcined at 650 °C in air.
[d] CL calcined at 400 °C in air.
[e] x is calculated after subtracting the oxygen from CuO reduction to Cu.
[f] H_2 consumption up to 580 °C.
[g] La-free, precipitated with ammonium carbonate.

ammonium carbonate (Table 2). The total hydrogen consumption is larger for the CP sample than for CL made by UGC, which might be due to the different structures formed during preparation by the CP and UGC techniques [11,22].

Regardless of the type of ceria or addition of metal, a peak at 700 °C corresponding to reduction of bulk oxygen of CeO_2, remains unchanged for all samples. This is similar to the case of Pt metals-on-ceria [7,43] or on ceria–zirconia oxide solid solutions [43]. Other transition metals and metal oxides on ceria have a similar effect [1,9,26,27,44]. In previous work, we found a clear reducibility enhancement of ceria by copper in the Cu–ceria system [1,9,26,44]. In this work, we have compared the reducibility of ceria induced by either the presence of gold or copper, as shown in Fig. 4B and Table 2. The reducibility is expressed by the value of "x" in CeO_x in Table 2. It should be noted that for the Cu-containing samples, the amount of hydrogen consumed is for reduction of both Cu_xO and ceria. The 10Cu–CL sample is much more reducible than the 5Cu–CL material. The effect of gold on ceria reducibility is stronger than that of Cu_xO. The peaks corresponding to the reduction of surface capping oxygen of ceria in the Au–ceria samples became much sharper and shifted to lower temperatures. The DP sample started to reduce around RT with a peak at 59 °C. Reduction on the UGC sample began at 80 °C with a peak at 110 °C. The peak area of the former was similar to the peak area of the corresponding Au-free ceria sample, as seen in Table 2. This suggests that most gold is in metallic state in this DP sample. However, the H_2 consumption over the UGC sample was higher than for the corresponding CL material, indicating the presence of oxidic gold.

H_2-TPR has been used in the literature to identify potentially higher oxidation states of gold on supports. Kang and Wan [32] reported that Au/Y-zeolite possessed two reduction peaks (at 125 and 525 °C) and one shoulder peak (at 190 °C). He attributed the first peak to oxygen adsorbed on the surface of metallic gold and the second to reduction of Au(III) located in sodalite cages. Neri et al. [45] reported two separated peaks (125 and 175 °C) for "as-prepared" Au/Fe_2O_3 without calcination. However, after oxidation at 300 °C, only one peak (165 °C) was observed. It was surmised that the first peak belongs to the reduction of Au oxide or hydroxide, which decomposes in calcination above 300 °C [13,14]. In Fig. 5 we note that all the profiles show more than one peak; contribution from oxidic gold reduction is possible, although it is masked by the much higher amount of ceria-oxygen. Based on the total hydrogen consumption, only the 0.9Au–CL (DP) (footnote 'b' in Table 2), the 3.8Au–CL (CP) and the 8Au–CL (UGC) samples (Table 2) appear to have an appreciable amount of oxidic gold, if we attribute the excess hydrogen consumption to oxidic gold reduction.

Fig. 5 clearly shows that gold facilitates the reduction of ceria surface oxygen species. With increasing gold loading, the reduction temperature shifted to lower temperatures for the DP samples. For instance, the 8.3Au–CL (DP) sample has two reduction peaks with peak temperature at 40 and 59 °C, while 0.9Au–CL (DP) has two reduction peaks with peak temperatures at 69 and 109 °C. The 4.5 and 8.3Au–CL (DP) samples have similar total peak areas, as shown in Fig. 5 and Table 2. However, the 0.9Au–CL (DP) sample shows higher hydrogen consumption, potentially due to

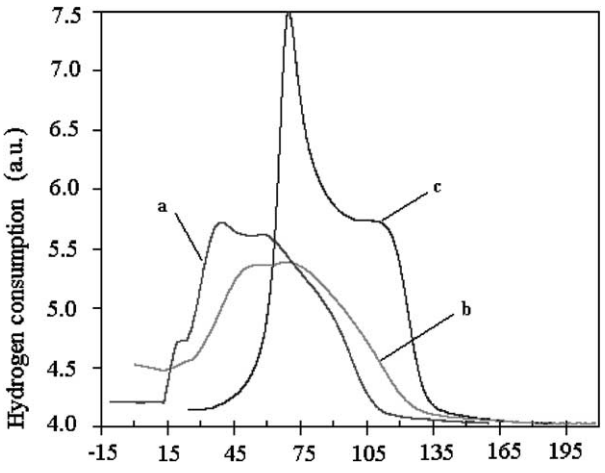

Fig. 5. H_2-TPR profiles of Au–ceria catalysts prepared by DP: (a) 8.3Au–CL (DP) (footnote 'c' in Table 1); (b) 4.7Au–CL (DP) (footnote 'c' in Table 1); (c) 0.9Au–CL (DP) (footnote 'c' in Table 1); 20% H_2/N_2, 50 cm^3/min (NTP), 5 °C/min. See Table 1 for sample identification and preparation conditions.

oxidic gold presence in this sample, as mentioned above. In general, addition of gold by the DP method drastically increases the oxygen reducibility of ceria.

Since the TPR technique is not as sensitive to surface oxygen titration, the effect of gold loading on the surface oxygen reducibility can be better followed by a step pulse titration technique effect**.** The use of CO at a constant temperature, to measure the oxygen availability is known as 'oxygen storage capacity'. The procedure involves creating a step change in the gaseous environment and under steady-state conditions monitoring the CO_2 produced.

In general, "oxygen storage" results from the change in oxidation state associated with the reversible removal and addition of oxygen:

$$2CeO_2 + CO \leftrightarrow Ce_2O_3 + CO_2,$$

$$2Ce_2O_3 + O_2 \rightarrow 4CeO_2$$

There are several techniques reported for measurements of OSC. Yao and Yu Yao [6] defined OSC as the value of O_2 uptake in each step pulse injection following a CO step pulse at equilibrium under the particular set of reaction conditions used. The total oxygen uptake for a series of O_2 step pulses following a series of CO injections until a constant breakthrough 95–98% was reached, was the measure of the cumulative oxygen storage capacity (OSCC) [6]. In other work, OSC was measured as the CO_2 formed during a CO step pulse after oxidation in O_2 [43]. Sharma et al. recently defined the OSC as the sum of CO_2 formed during a CO step pulse and an O_2 step pulse after the CO step pulse [46].

OSC measurements involve a dynamic reaction process. Therefore, OSC is influenced by several operating parameters: pretreatment temperature, temperature during the pulsing experiment, the concentration of gaseous reactant, and the presence of precious metals.

The presence of a precious metal facilitates both the restoration of the surface oxygen anions and their removal by CO at lower temperatures [6,43,46]. Increasing the surface area was found to enhance the OSC of ceria-based catalysts [47]. Moreover, decreasing the CeO_2 crystallite size leads to greater metal–ceria interaction as shown by both TPR and OSC measurements of the Pt metal-loaded ceria [43].

In this work, we examined the effect of the presence of gold and copper on the OSC of ceria. Results from step pulse measurements at 350 °C with 10% CO/He and 10% O_2/He at 50 cm^3/min flow rate on 8Au–CL (UGC) and CL (UGC) are shown in Fig. 6. The data have been corrected by subtraction of background signals. The preoxidized CL sample was exposed to two-step pulses of CO followed by two-step pulses of O_2. For the first CO step, a significant amount of CO_2, 284.4 μmol/g_{cat} was formed. Over the Au–ceria sample, a much higher amount of CO_2 was measured during the first CO step (Fig. 6). Negligible CO_2 was produced during the second step pulse of CO on either sample.

It is noted that three minutes in CO under these conditions are not enough to remove all available oxygen from ceria. The kinetics of the process at 350 °C is very slow. The CO_2 produced consists of a sharply rising edge due to rapid reaction of CO with the surface oxygen, followed by a plateau and a long decreasing edge, which is attributed to reaction of CO with the bulk oxygen of ceria whose availability is limited by diffusion. It should be noted that the straw color of stoichiometric ceria immediately changed into the dark blue-gray color of reduced cerium oxide upon exposure to CO. In the oxygen step pulse, over the reduced Au–ceria sample, a very sharp CO_2 spike of 348.5 μmol/g_{cat} was observed (Fig. 6). The small peak of CO seen during the O_2 step pulse is part of the fragmentation pattern of CO_2 in the mass spectrometer. The same observation was made by Sharma et al. [46] in their OSC measurements of Pd–ceria. In that paper, the authors proposed that this CO_2 spike is due to desorption of CO_2 adsorbed during the initial CO step on Ce^{3+} sites. This CO_2 is then displaced when ceria is reoxidized during the O_2 pulse. On the basis of this interpretation, the total amount of CO_2 formed in the CO step is the sum of the CO_2 formed in both events. However, other interpretations, such as the oxidation of carbon deposited from CO disproportionation [47], have also appeared in the literature.

For the samples examined in this work, Fig. 7a shows the CO_2 production measured at three different temperatures, during the first CO step for 8Au–CL (UGC), 5Cu–CL (UGC), 10Cu–CL (UGC), 4.5Au–CL (DP), and CL (UGC) samples. These samples were selected because they have similar surface areas (see Table 1). At 100 °C, the OSC of 8Au–CL (UGC) is 259.6 μmol/g_{cat}, while that of CL and pure ceria is zero. At 200 °C, the OSC of 8Au–CL (UGC) is to 327.6 μmol/g_{cat}, while that of CL is 48.4 μmol/g_{cat}. Similarly, the OSC of the other catalysts is higher compared to that of CL at all three temperatures. As also found by H_2-TPR, the OSC measurements below 350 °C provide

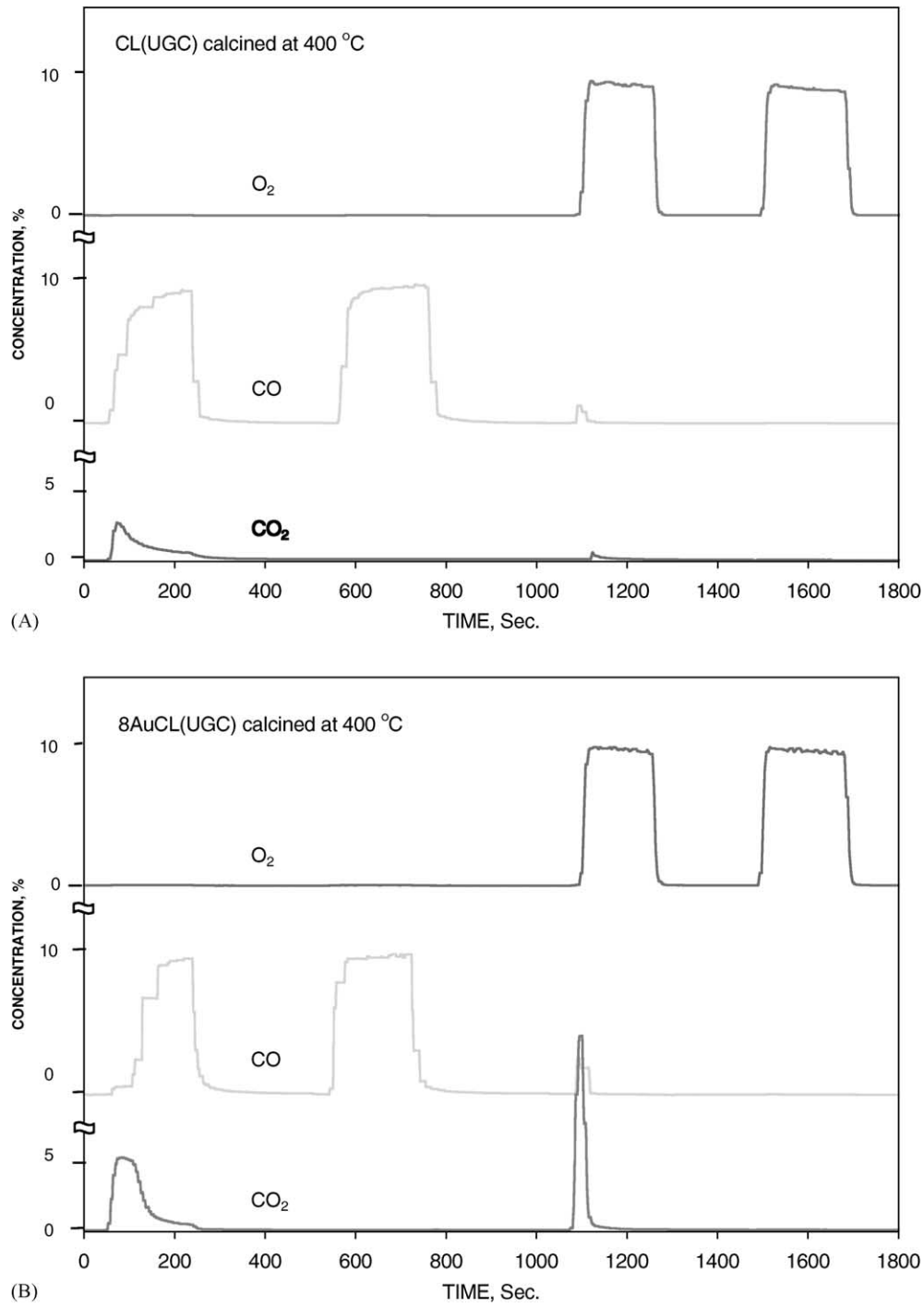

Fig. 6. OSC of (A) CL (UGC) and (B) 8Au–CL (UGC) calcined at 400 °C, 10% CO/He and 10% O_2/He, 50 cm^3/min (NTP), 350 °C.

evidence that the surface oxygen of ceria is greatly weakened by the addition of gold and copper. The present data demonstrate the importance of the kinetics of oxygen incorporation and removal in the composite ceria structure.

The CO_2 production during the first O_2 step is shown in Fig. 7b. All samples display this, including the metal-free ceria. The amount of CO_2 eluted at 350 °C is similar for all samples. At lower temperatures, however, the Au–ceria samples show the highest amount of CO_2. This may be viewed as a consequence of their more reduced (Ce^{3+}) state achieved during the preceding CO step.

The oxidation of reduced ceria by water was examined at 350 °C on 4.5Au–CL (DP) as shown in Fig. 8. An amount of 180.9 μmol/g_{cat} CO_2 was produced during the H_2O step. This was accompanied by a similar amount of H_2 (180.3 μmol/g_{cat}). Thus, H_2O is dissociated in the process.

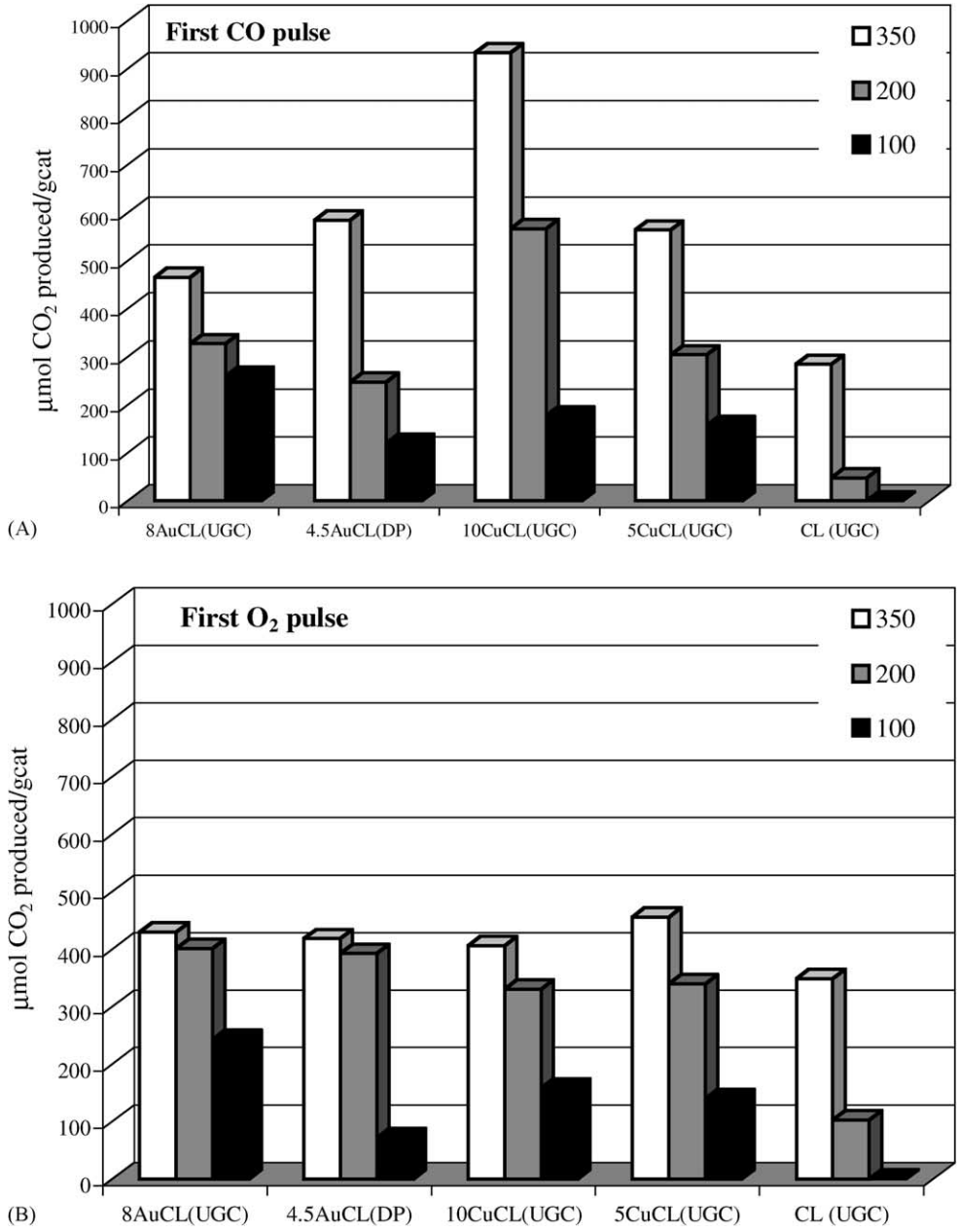

Fig. 7. OSC of ceria-based catalysts at three different temperatures 100, 200 and 350 °C; 10% CO/He, 10% O_2/He, 50 cm^3/min (NTP), all materials calcined at 400 °C, 10 h.

However, carbon-containing species cannot be fully removed by H_2O. Additional CO_2 (114.8 µmol/g_{cat}) is eluted in the subsequent O_2 step (Fig. 8). This finding may be used to explain why carbon-containing species were detected by FT-IR during in situ water-gas shift [48].

3.3. Activity studies

Fig. 9 shows steady-state CO conversions over 8Au–CL (UGC), 10Cu–CL (UGC), 5Cu–CL (UGC), 4.5Au–CL (DP), and CL (UGC) in a feed gas of 2% CO/10% H_2O/He. These are the same samples examined by H_2-TPR (Fig. 4B) and OSC measurements (Fig. 8), chosen on the basis of similar surface area. The WGS light-off temperature of all metal-modified ceria samples is below 120 °C, while ceria itself is inactive below 300 °C. At 200 °C, the 8Au–CL (UGC) sample shows the highest reactivity, in agreement with the OSC data of Fig. 8. One may explain the lower activity of the 5Cu–CL (UGC) sample by the fact that it is only partially reduced at 200 °C, as shown in Fig. 4B, and Table 2. However, the activity of 10Cu–CL (UGC) is not as high as what would be predicted on the basis of the TPR data. On the other hand, the OSC values, after subtraction of the CuO contribution, become much lower (617.2 µmol/g_{cat})

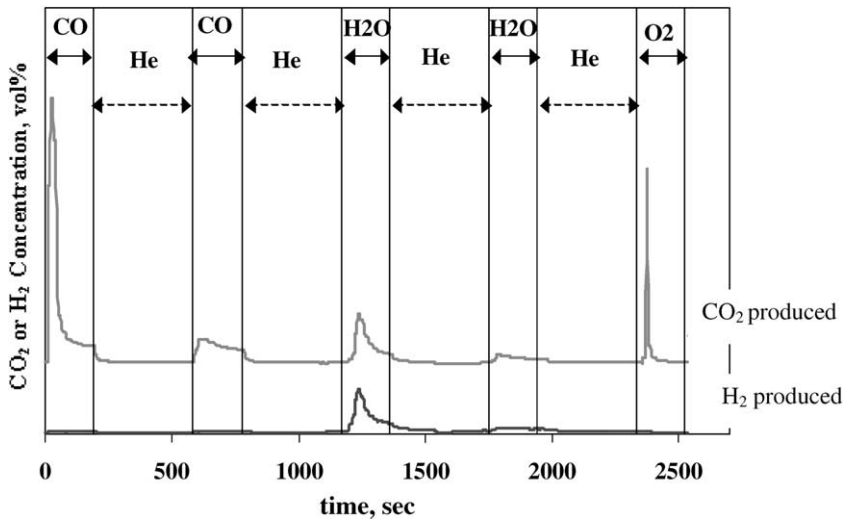

Fig. 8. CO–H_2O–O_2 pulse measurement on 4.5Au–CL (DP) (footnote 'f' in Table 1) catalysts at 350 °C; 10% CO/He, 3% H_2O/He, 10% O_2/He, 50 cm^3/min (NTP).

than for the 8Au–CL (UGC) sample (Fig. 8). The extent of CuO reduction at each temperature is not known, however. Additional structural investigations are needed to elucidate further the metal–ceria interaction and its relevance to the WGS reaction.

Preliminary rate measurements indicate that a key parameter for WGS activity is the particle size of ceria [11,28]. As identified here by XPS, Au is present both in metallic as well as in oxidized state in the Au–CL catalysts. We do not know whether one or both of these states are important in WGS. What we know at the present time is that the presence of gold is crucial for the reaction to occur at low temperatures on ceria. The cooperative redox mechanism, whereby CO is adsorbed on gold sites, while oxygen is supplied by ceria is plausible, but needs to be supported by spectroscopic studies. Also, the effect of H_2 and CO_2 on the reaction rate needs to be evaluated. Such studies are currently underway in our laboratory.

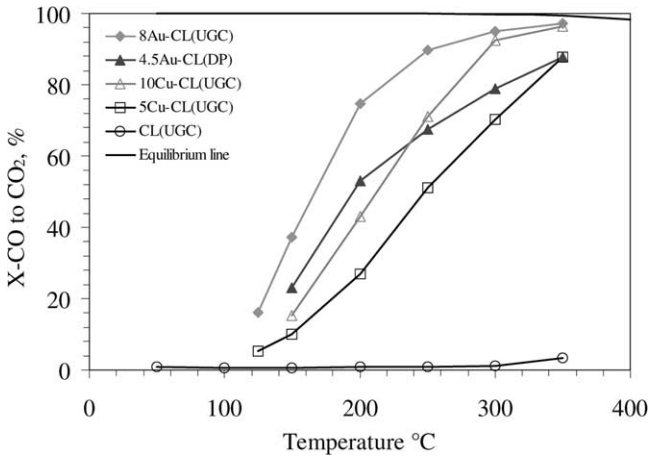

Fig. 9. WGS activity of various ceria-based materials calcined at 400 °C, 10 h, 2% CO/10.7% H_2O/He, 0.09 g s/cm^3 (NTP) (GHSV = 80,000 h^{-1}).

During a 120 h long stability test of the 4.7Au–CL (DP) sample (footnote 'c' in Table 1), its catalytic activity remained the same in a reformate type gas mixture containing 7% CO/38% H_2O/11% CO_2/33% H_2/He at 300 °C (space velocity 6000 h^{-1}). No significant changes were observed in the conversion of CO (around 60%) during this test period. Catalyst characterization after this test, found that the ceria particle size increased only slightly, while the gold particle size grew to 6.7 nm (Table 1).

4. Conclusion

Au–ceria is an active and stable catalyst for WGS reaction in the temperature range 150–350 °C. Addition of Au improves the reducibility and the OSC of cerium oxide. The amount of surface oxygen available for reduction is controlled primarily by the crystal size of ceria. The presence of gold is crucial, however, in that it greatly weakens this oxygen and facilitates the interaction with CO at lower temperatures. The active site of gold in WGS over Au–ceria catalysts is not known. Several of the samples examined in this work show the presence of gold ions, in addition to metallic gold. Differences in WGS activity between Cu–ceria and Au–ceria at temperatures below 200 °C warrant further investigation.

Acknowledgements

The financial support of this work by NSF/EPA, Grant #CTS-9985305, is gratefully acknowledged. QF also thanks Mr. Steve Fiore for his help with the OSC measurements.

References

[1] Y. Li, Q. Fu, M. Flytzani-Stephanopoulos, Appl. Catal. B: Environ. 27 (2000) 179.
[2] T. Bunluesin, R.J. Gorte, Appl. Catal. B: Environ. 15 (1998) 107.
[3] T. Shido, Y. Iwsawa, J. Catal. 141 (1993) 71.
[4] J.Z. Shyu, K. Otto, W.L.H. Watkins, G.W. Graham, R.K. Belitz, H.S. Gandhi, J. Catal. 23 (1988) 114.
[5] M.G. Sanchez, J.L. Gazquez, J. Catal. 104 (1987) 120.
[6] H.C. Yao, Y.F. Yu Yao, J. Catal. 86 (1984) 254.
[7] A. Trovarelli, Catal. Rev.-Sci. Eng. 38 (1996) 439.
[8] M. Haruta, Catal. Today 29 (1997) 153.
[9] W. Liu, M. Flytzani-Stephanopoulos, J. Catal. 53 (1995) 304–332.
[10] H. Sakurai, A. Ueda, T. Kobayashi, M. Haruta, Chem. Commun. (1997) 271.
[11] Q. Fu, A. Weber, M. Flytzani-Stephanopoulos, Catal. Lett. 77 (1–3) (2001) 87.
[12] Y. Yuan, K. Asakura, H. Wan, K. Tsai, Y. Iwasawa, J. Catal. 170 (1997) 191.
[13] M. Haruta, N. Yamada, T. Kobayashi, S. Iijima, J. Catal. 115 (1989) 301.
[14] M. Haruta, S. Tsubota, T. Kobayashi, J. Kageyama, M.J. Genet, B. Delmon, J. Catal. 144 (1993) 175.
[15] D. Andreeva, V. Idakiev, T. Tabakova, A. Andreev, J. Catal. 158 (1996) 354.
[16] S. Gardner, G. Hoflund, D. Schryer, J. Schryer, B. Upchurch, E. Kielin, Langmuir 7 (1991) 2135.
[17] A. Ueda, T. Oshima, M. Haruta, Appl. Catal. B: Environ. 12 (1997) 81.
[18] S.D. Lin, M. Bollinger, M.A. Vannice, Catal. Lett. 17 (1993) 245.
[19] M. Valden, X. Lai, D.W. Goodman, Science 281 (1998) 1647.
[20] K.J. Choi, B.Y. Coh, H.I. Lee, Catal. Today 44 (1998) 205.
[21] T. Tabakova, V. Idakiev, D. Andreeva, I. Mitov, Appl. Catal. A: Gen. 202 (2000) 91.
[22] A. Weber, M.S. Thesis, Department of Chemical Engineering, Tufts University, Medford, MA, 1999.
[23] Q. Fu, Y. Li, A. Weber, M. Flytzani-Stephanopoulos, in: Proceedings of the 2000 Annual AIChE Meeting, Paper #41f, Los Angeles, CA, 12–17 November 2000.
[24] S. Tsubota, D.A.H. Cunningham, Y. Bando, M. Haruta, in: G. Poncelet, et al. (Eds.), Preparation of Catalysts VI, Elsevier, Amsterdam, 1995, 275 pp.
[25] J.W. Niemantsverdriet, Spectroscopy in Catalysis, VCH, New York, NY, 1995.
[26] Lj. Kundakovic, M. Flytzani-Stephanopoulos, Appl. Catal. A: Gen. 171 (1998) 13.
[27] Lj. Kundakovic, M. Flytzani-Stephanopoulos, J. Catal. 179 (1998) 203.
[28] Q. Fu, Ph.D. Dissertation, Tufts University, in progress.
[29] C. Sze, E. Gulari, B.G. Demczyk, Mater. Lett. 36 (1998) 11.
[30] Y.M. Kang, B.Z. Wan, Appl. Catal. A: Gen. 128 (1) (1995) 53.
[31] M. Haruta, T. Kobayashi, S. Iijima, F. Delannay, in: M.J. Phillips, M. Ternan (Eds.), Proceedings of the Ninth International Congress on Catalysis, Vol. 2, Calgary, The Chemical Institute of Canada, Ottawa, 1988, p. 1206.
[32] Y.M. Kang, B.Z. Wan, Catal. Today 35 (1997) 379.
[33] A.I. Kozlov, A.P. Kozlova, H. Liu, Y. Iwasawa, Appl. Catal. A: Gen. 182 (1999) 9.
[34] A.M. Visco, F. Neri, G. Neri, A. Donato, C. Milone, S. Galvagno, Phys. Chem. Chem. Phys. 1 (1999) 2869.
[35] F.E. Wagner, S. Galvagno, C. Milone, A.M. Visco, L. Stievano, S. Calogero, J. Chem. Soc., Faraday Trans. 93 (1997) 3403.
[36] E.D. Park, J.S. Lee, J. Catal. 186 (1999) 1.
[37] M. Haruta, T. Takase, T. Kobayashi, in: S. Yoshida, et al. (Eds.), Catalysis Science and Technology, Vol. 1, Kodansha, Tokyo, 1999, 331 pp.
[38] F. Boccuzzi, A. Chiorino, J. Phys. Chem. B 104 (2000) 5414.
[39] W.S. Epling, G.B. Hoflund, J.F. Weaver, S. Tsubota, M. Haruta, J. Phys. Chem. 100 (1996) 9929.
[40] Y.M. Chiang, E.B. Lavik, I. Kosacki, H.L. Tuller, J.Y. Ying, J. Electroceram. 1 (1997) 7.
[41] A. Trovarelli, C. de Leitenburg, G. Polcetti, J. Llorca, J. Catal. 151 (1995) 111.
[42] G. Groppi, C. Cristiani, L. Lietti, C. Ramella, M. Valentini, P. Forzatti, Catal. Today 50 (1999) 399.
[43] H.W. Jen, G.W. Graham, W. Chun, R.W. McCabe, J.P. Cuif, S.E. Deutsch, O. Touret, Catal. Today 50 (1999) 309.
[44] W. Liu, M. Flytzani-Stephanopoulos, Chem. Eng. J. 64 (1996) 283.
[45] G. Neri, A.M. Visco, S. Galvagno, A. Donato, M. Panzalorto, Therm. Acta 329 (1999) 39.
[46] S. Sharma, S. Hilaire, J.M. Vohs, R.J. Gorte, H.-W. Jen, J. Catal. 190 (2000) 199.
[47] A. Holmgren, B. Andersson, D. Duprez, Appl. Catal. B: Environ. 22 (1999) 215.
[48] S. Hilaire, X. Wang, T. Luo, R. Gorte, J. Wagner, Appl. Catal. A: Gen. 215 (2001) 271.